Journal of Zhejiang University-SCIENCE C (Computers & Electronics)
ISSN 1869-1951 (Print); ISSN 1869-196X (Online)
www.zju.edu.cn/jzus; www.springerlink.com
E-mail: jzus@zju.edu.cn

A power conversion system for PMSG-based WECS operating with fully-controlled current-source converters*

Jian-yu BAO†[1], Wei-bing BAO[2], Yu-ling LI[3]

([1]*Ningbo Institute of Technology, Zhejiang University, Ningbo 315100, China*)

([2]*Zhijiang College, Zhejiang University of Technology, Hangzhou 310024, China*)

([3]*College of Electrical Engineering, Zhejiang University, Hangzhou 310027, China*)

†E-mail: baojy@nit.zju.edu.cn

Received Aug. 26, 2013; Revision accepted Nov. 13, 2013; Crosschecked Feb. 19, 2014

Abstract: We propose a new power conversion system for a permanent magnet synchronous generator (PMSG) based grid-connected wind energy conversion system (WECS) operating with fully-controlled back-to-back current-source converters. On the generator side, two independent current-source rectifiers (CSRs) with space-vector pulse width modulation (SVPWM) are employed to regulate and stabilize DC-link currents. Between DC-link and the electrical grid, a direct-type three-phase five-level current-source inverter (CSI) is inserted as a buffer to regulate real and reactive power fed to the grid and thus adjusts the grid side power-factor. We also present a current-based maximum power point tracking (MPPT) scheme, which helps the generator extract the maximum power through closed-loop regulation of the generator speed. By applying the multilevel modulation and control strategies to the grid-side five-level CSI, a multilevel output current waveform with less distortion is produced, and the bulk requirement of the output capacitor filter to eliminate the harmonic current is reduced. All the proposed concepts are verified by simulation models built in a PSIM environment.

Key words: Grid-connected, Wind energy conversion, Current-source rectifier, Multilevel current-source inverter
doi:10.1631/jzus.C1300231 **Document code:** A **CLC number:** TM4

1 Introduction

Fully-controlled power converters have attractive choices and are used as power interfaces between the synchronous generator and grid for a direct-drive wind turbine (WT) based wind energy conversion system (WECS). In the current WECS, the mostly used topologies are matrix converters, two-level and multilevel voltage-source converters (VSCs) (Melício *et al.*, 2011). The whole system is usually configured into the back-to-back connected structure. The generator-side converter is used to achieve the maximum power point tracking (MPPT). The grid-side converter is not only actively controlled to meet the harmonics and power factor demands (Singh *et al.*, 2011), but also required to supply the reactive or real power to the grid loads (Sharma and Singh, 2012; Alizadeh and Yazdani, 2013). However, for VSC based WECS, a DC-DC converter is usually added to boost DC-link voltage due to its inherent buck characteristics. Thus, the cost and complexity of the conversion system must be considered. The current-source converter (CSC), as the dual part of VSC, is less popular than the VSC in commercial applications because of the lower energy storage efficiency of the inductors (Sahan *et al.*, 2011). CSC has certain advantages, such as inherent boost and short-circuit protection capabilities, direct control of the output current, longer lifetime of the storage unit, and flexible power flow control. Thus, CSC has recently drawn considerable attention for energy con-

* Project supported by the National Natural Science Foundation of China (No. 51277164) and the Natural Science Foundation of Zhejiang Province, China (No. Y1111002)

version applications.

Nowadays, a few CSC based configurations have been applied in permanent magnet synchronous generator (PMSG) based WECS. Dai *et al.* (2009) proposed the configuration of a thyristor rectifier plus thyristor inverter, in which the trigger angle of the thyristor rectifier is used to provide MPPT control. By using a diode rectifier in place of a thyristor rectifier, Wang *et al.* (2011) proposed the configuration of a diode rectifier plus a semi-controlled thyristor inverter, in which MPPT control and the optimum DC-link current regulation are implemented by regulating the firing angle of the thyristor inverter. Teshirogi and Nishikata (2011) investigated the effects of various system parameters on the performance characteristics of a wind turbine generating system using a current source thyristor inverter. However, using a thyristor converter for grid-connected applications will cause the power factor and harmonic performance to be degraded. Nikolic and Jeftenic (2010) proposed the approach of pulse width modulation (PWM) controlled symmetrical gate commutated thyristors (SGCTs). By controlling the inverter modulation index, the DC-link current is kept at a minimum value with various wind speeds and thus reduces the converter power loss at lower power levels. Using the multilevel power converter topologies in WECS can improve the power quality injected into the electrical grid (Melício *et al.*, 2010; Senturk *et al.*, 2012). For a CSC based configuration, there are mainly two converter topologies to generate multilevel output-current waveform: one is a multimodule CSC connected in parallel (Bai *et al.*, 2013), and the other uses cascaded PWM CSCs at both the generator and grid sides (Popat *et al.*, 2012b). Moreover, Popat *et al.* (2012a; 2013) investigated and studied some practical applications such as the coordinated control scheme for the whole PMSG based wind farm, DC-link current balancing regulation, and fault ride-through capability.

In this study, a new configuration for PMSG based grid-connected WECS operating with fully-controlled back-to-back CSCs is proposed, and the operational principle of such a configuration is investigated. On the generator side, two independent current-source rectifiers (CSRs) with space-vector pulse width modulation (SVPWM) are employed to regulate and stabilize the DC-link current, and the MPPT scheme is implemented through a closed-loop regulation of generator speed. Between DC-link and the electrical grid, a direct-type three-phase five-level current-source inverter (CSI) is inserted as a buffer to regulate active and reactive power flowing to the grid, by applying the multilevel modulation and control strategies to the grid-side five-level CSI. The filtering circuit is relatively easy to implement due to the increased equivalent switching frequency of the inverter. The current injected into the grid is with less harmonic distortion. All the proposed concepts are verified by simulation models built in a PSIM environment.

2 System configuration

The circuit configuration of a fully-controlled back-to-back CSC used for WECS is shown in Fig. 1. The whole system consists of a low speed PMSG, two identical fully-controlled CSRs, DC-link reactors, and a direct-type three-phase five-level CSI. Both CSR and multilevel CSI employ the insulated gate bipolar transistor (IGBT). A fat-recovery diode is connected in series with each IGBT. These two CSRs generate two independent DC current sources, which will be directly supplied to the proposed five-level CSI. The five-level CSI is configured as a power interface to flexibly regulate active and reactive power between the wind generator and electrical grid. The grid is modeled as a voltage-source in series with little source-impedance (L_o and R_o). L_o represents the sum of line impedance and leakage inductance of the transformer, while R_o is referred to as the transformer and line loss.

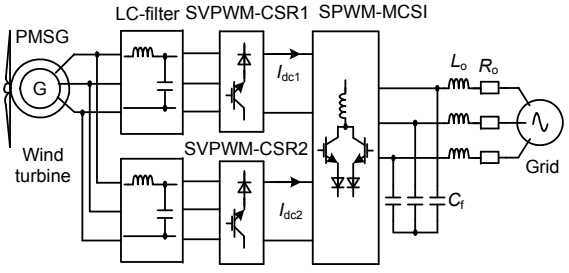

Fig. 1 Circuit configuration of CSC based WECS

3 Operation of generator-side CSR

To capture the maximum power from the wind turbine, a current based MPPT scheme is implemented through the closed-loop regulation of the generator speed. The maximum power available at a certain wind speed can be achieved at a controllable DC-link current via a speed loop regulation. According to the MPPT controller, the optimum speed of the generator is obtained and fed to the speed loop controller as the reference value, and the rotating speed of PMSG follows the reference speed to capture the maximum power from WT via a simple proportional-integral (PI) regulator.

Fig. 2 shows the block diagram of the SVPWM control of the CSR, which is implemented based on a field oriented *d*-*q* synchronous rotational frame. By applying *abc*-*dq* transformation with synchronizing angle θ_r, three-phase output currents from PMSG are converted into *d*- and *q*-axis time-invariant current components, which are labeled as i_{dr} and i_{qr}, respectively. Similar to a permanent magnet synchronous motor (PMSM) control, i_{dr} represents the reactive current component and i_{qr} acts as the active current component. Two PI regulators are applied to control i_{dr} and i_{qr}, respectively. The active current reference i_{qr_ref} is obtained from the speed regulator, and the reactive current reference i_{dr_ref} is usually set to zero to obtain the unity power factor at the generator side. The deviations of *d*- and *q*-axis current components are fed to the PI regulators. By moderate adjustment, *d*- and *q*-axis current components follow their corresponding given value via gating the switches of CSR properly.

The current based SVPWM (Dupczak *et al.*, 2012) is used to generate the switching gate signals of the CSR. Different from the voltage space vector, a three-phase CSR has six active states and three zero states, as shown in Fig. 3. By finding the mapping relationship between the voltage vectors and current vectors, the dwell times of the current vectors at different sectors are determined by the combination of Eq. (1) and Table 1. The periodical interval for sampling the reference current vector is set to T_s, and the reference current vector is synthesized by two active vectors and a zero vector in each sector. T_1 and T_2 represent the duration times of the six active vectors at different sectors, and T_0 represents the duration time of the three zero vectors.

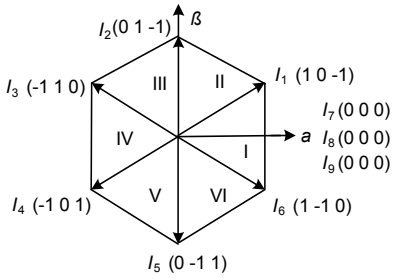

Fig. 3 Current vectors of three-phase CSR

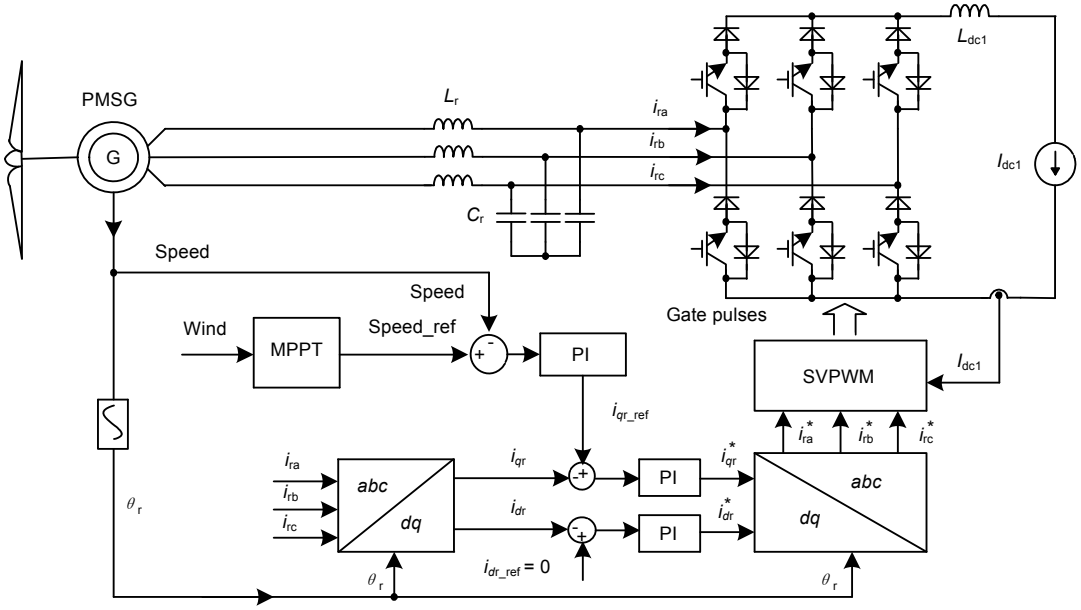

Fig. 2 An SVPWM CSR combined with MPPT

$$\begin{cases} X = \dfrac{T_s}{2I_{dc}}(I_\alpha + \sqrt{3}I_\beta), \\ Y = \dfrac{T_s}{2I_{dc}}(I_\alpha - \sqrt{3}I_\beta), \\ Z = \dfrac{T_s}{I_{dc}}I_\alpha, \\ T_0 = T_s - T_1 - T_2, \end{cases} \quad (1)$$

where I_{dc} is DC output current from CSR, and I_α and I_β are obtained through *abc*-$\alpha\beta$ transformation.

Table 1 Duration times of current vector at six sectors

Sector	I	II	III	IV	V	VI
T_1	Y	Z	X	$-Y$	$-Z$	$-X$
T_2	X	$-Y$	$-Z$	$-X$	Y	Z

4 Operation of the grid-side five-level CSI

To achieve a lower distortion of the output currents, a direct-type three-phase five-level CSI composed of fully controllable devices is applied on the grid side. This five-level CSI topology is obtained from the improved three-phase flying-capacitors five-level voltage source inverter (VSI) through dual transformation (Bao *et al.*, 2010a; 2010b) and two independent current-sources are needed. The proposed three-phase five-level CSI topology is shown in Fig. 4.

4.1 Generation mechanism of five current levels

With the assumption that DC current-sources I_1 and I_2 are equal to $2I_{dc}$, the currents flowing through the sharing-inductors are all equal to I_{dc}. The operational modes for generating three current levels of i_{a1} can be obtained as follows:

1. A_S_{p1}, A_S_{p2}, and A_S_{c2} are on, $i_{a1}=+2I_{dc}$;

2. (A_S_{p1}, A_S_{n2}, A_S_{c1}) or (A_S_{p2}, A_S_{n1}, A_S_{c2}) are on, $i_{a1}=+I_{dc}$;

3. A_S_{n1}, A_S_{n2}, and A_S_{c1} are on, $i_{a1}=0$.

In a similar way, three current levels of i_{b1} can be generated as follows:

1. B_S_{p1}, B_S_{p2}, and B_S_{c2} are on, $i_{b1}=+2I_{dc}$;

2. (B_S_{p1}, B_S_{n2}, B_S_{c1}) or (B_S_{p2}, B_S_{n1}, B_S_{c2}) are on, $i_{b1}=+I_{dc}$;

3. B_S_{n1}, B_S_{n2}, and B_S_{c1} are on, $i_{b1}=0$.

The total output current of phase-a is i_a, which is generated by i_{a1} minus i_{b1}. While i_{a1} and i_{b1} have three current levels respectively, by subtraction with each other, i_a can generate five current levels: $+2I_{dc}$, $+I_{dc}$, 0, $-2I_{dc}$, and $-I_{dc}$. In the same way, i_b and i_c can generate five current levels, respectively.

4.2 Phase-disposition (PD) PWM implementation

The PD-PWM strategy applied in a multilevel VSI can lower line-to-line harmonic distortion. The proposed five-level CSI is obtained by dual transformation from the generalized five-level VSI. Thus, this generalized five-level CSI can also be PD-PWM

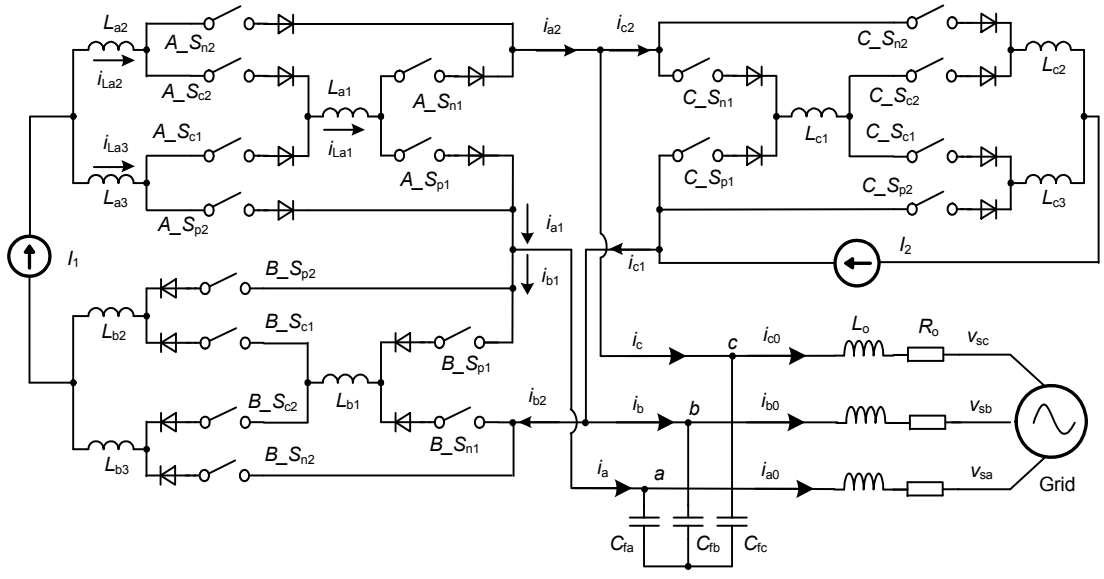

Fig. 4 Proposed three-phase five-level CSI

controlled to produce the same harmonic performance for three-phase output currents. According to the generation mechanism of five current levels described above, two in-phase triangular carriers and three-phase fundamental reference waveforms are arranged as shown in Fig. 5. When the reference waveforms are compared against the upper triangular carrier W_{C1}, the phase leg outputs switch between $+2I_{dc}$ and $+I_{dc}$, while when they are compared against the lower triangular carrier W_{C2}, the phase leg outputs switch between $+I_{dc}$ and 0. Table 2 lists the decoded switching states for generating three current levels of i_{a1}.

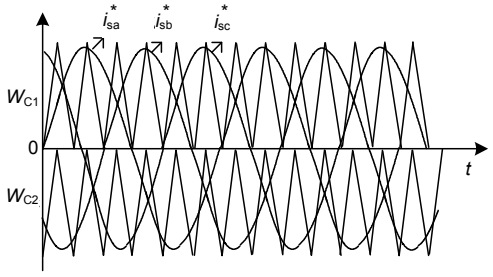

Fig. 5 Carrier and modulation waveforms of PD-PWM

Table 2 Switching states for three-level PD-PWM

i^*_{sa}	Comparison	Conducting switches	i_{a1}
$i^*_{sa}>0$	$i^*_{sa}>W_{C1}$	$A\_S_{p1}, A\_S_{p2}, A\_S_{c2}$	$+2I_{dc}$
	$i^*_{sa}<W_{C1}$	$A\_S_{p1}, A\_S_{n2}, A\_S_{c1}$ $A\_S_{p2}, A\_S_{n1}, A\_S_{c2}$	$+I_{dc}$
$i^*_{sa}<0$	$\lvert i^*_{sa}\rvert<\lvert W_{C2}\rvert$	$A\_S_{p1}, A\_S_{n2}, A\_S_{c1}$ $A\_S_{p2}, A\_S_{n1}, A\_S_{c2}$	$+I_{dc}$
	$\lvert i^*_{sa}\rvert>\lvert W_{C2}\rvert$	$A\_S_{n1}, A\_S_{n2}, A\_S_{c1}$	0

4.3 Grid-connected control

For a multilevel CSI-based WECS, AC currents from the CSI inverters injected into the grid are expected to be sinusoidal, and the active and reactive power injected into the grid can be adjusted independently according to the system requirement. Similar to the grid-connected control for VSI, the grid-connected control for a multilevel CSI-based WECS can also be implemented based on a grid voltage oriented synchronous frame.

As illustrated in Fig. 6, the PWM and control of the five-level CSI need to be synchronized to the grid voltage through a phase-locked loop (PLL) (Chung, 2000). With the obtained synchronizing angle θ_s, three-phase line currents are projected into a *d*-*q* synchronous frame. The *d*- and *q*-axis current components are obtained, labeled as i_{sd} and i_{sq} respectively. The error signals between the reference command I^*_{sd} and i_{sd}, and the reference command I^*_{sq} and i_{sq}, are processed by two PI controllers to generate the modulating signals. Through *dq*-to-*abc* transformation, three-phase sinusoidal current reference signals i^*_{sa}, i^*_{sb}, and i^*_{sc} are obtained from m_d and m_q, which are acted as three-phase modulation signals to implement PD-PWM as illustrated in Fig. 5.

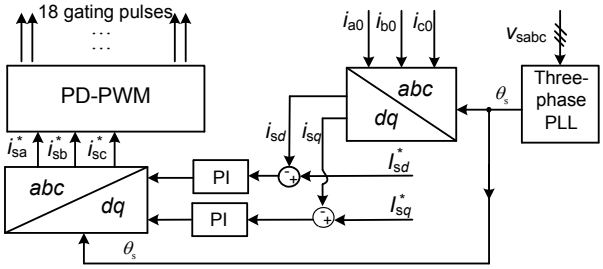

Fig. 6 Grid-connected control scheme

The reference commands I^*_{sd} and I^*_{sq} are used to adjust the real power and reactive power injected into the grid, respectively. To simplify the analysis, power control of this five-level CSI is based on a grid voltage oriented synchronous frame. Thus, three-phase grid voltages are decomposed into *d*- and *q*-axis voltage components through an *abc*-to-*dq* transformation, while the *q*-axis voltage component v_{sq} is usually regulated to zero through a PI controller. So, the grid voltage has only a *d*-axis voltage component v_{sd} if the *d*-axis is aligned to the voltage phasor. The *d* and *q* subscriptions of the following variables represent *d*- and *q*-axis components of the corresponding variable, respectively. In a *d*-*q* synchronous frame, if v_{sq} is equal to zero, the active or reactive power will have no relation to v_{sq}. Therefore, the expressions of the active power P_s and the reactive power Q_s can be greatly simplified as shown in Eq. (2) (Dash and Kazerani, 2011):

$$\begin{cases} P_s = 1.5 v_{sd} i_{sd}, \\ Q_s = 1.5 v_{sd} i_{sq}, \end{cases} \tag{2}$$

where P_s is proportional to i_{sd}, and Q_s is proportional to i_{sq}. Similarly, P_s and Q_s can be controlled by i_{sd} and

i_{sq}, respectively. Therefore, in this WECS, the active and reactive powers are independently controlled through giving the values of *d*- and *q*-axis reference currents I_{sd}^* and I_{sq}^*. By setting I_{sd}^* to a positive value, and letting $I_{sq}^*=0$, the unity power factor will be achieved on the grid side. If a positive value is given to I_{sq}^*, then the leading displacement power factor will be produced on the grid side. Similarly, the lagging displacement power factor will occur when a negative value is given to I_{sq}^*.

5 Simulation analysis

To validate the operations of CSCs used for PMSG based WECS, a simulation model composed of fully controllable current source converters was constructed and simulation results were analyzed via PSIM. The major system parameters of the proposed WECS are listed in Table 3. All the active semiconductor switches used in generator-side CSR and grid-side five-level CSI are made up by using IGBTs in series with fast recovery diodes.

Table 3 Major parameters of the proposed WECS

System parameter	Value
Power	2.5 MW
Voltage (line-to-line)	735 V
Current	2000 A
Frequency	50 Hz
Rated wind speed	12 m/s
Number of pole pairs	56
Base frequency	10 Hz
L_d (*d*-axis inductance)	0.00197 H
L_q (*q*-axis inductance)	0.00303 H
Switching frequency (CSR)	1050 Hz
Switching frequency (CSI)	1050 Hz

5.1 Simulation analysis on the generator side

In Fig. 7, the top subplot shows the waveform of the gradient wind speed. The initial speed is 9 m/s, and the speed is gradually raised to 12 m/s at *t*=3 s. According to the varying wind speed, the MPPT module calculates the maximum power which can be extracted from WT. The maximum power P_{max} is shown in the middle subplot. $P_{turbine}$, shown in the bottom subplot, is the actual output power from WT, which varies with the actual wind speed, and follows P_{max} well via MPPT regulation.

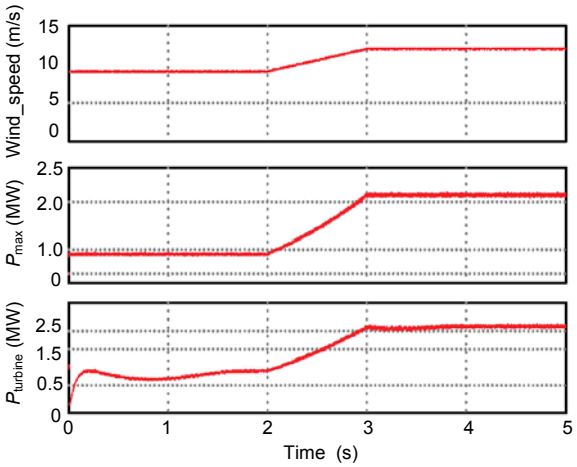

Fig. 7 Wind speed and power

Fig. 8 shows how MPPT works with the varying wind speed. The faster the wind speed, the higher the power generated to obtain the maximum power from WT. The MPPT module calculates the optimal rotation speed for PMSG by sampling the varied wind speed (shown in the top subplot). The second subplot shows the optimal rotation speed of PMSG, which is also the reference value used for the speed closed-

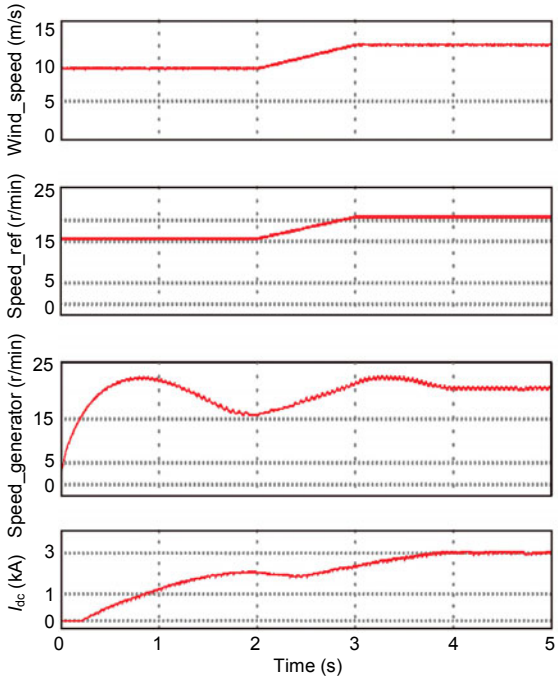

Fig. 8 Wind, generator speed, and DC-link current

loop regulation. The actual generator speed is shown in the third subplot, to capture the maximum power from WT, which follows the reference speed well via the PI regulation. The AC output voltage from PMSG is converted into DC current by SVPWM CSR. The obtained DC-link current I_{dc} is shown in the bottom subplot, which is controllable with the varying wind speed through the MPPT control. Therefore, accompanied with the varied wind speed, the DC-link current will change accordingly, and thus will affect the total power transferred to the grid.

5.2 Simulation analysis on grid side

The waveforms shown in Fig. 9 are: five-level PWM output current of CSI, line current and grid voltage, power factor, and active power output. The wind speed between 0 s and 2.5 s is 9 m/s. When the wind speed is stable, the DC-link output current is also stable. Three-phase five-level CSI is supplied with this DC-link current. The five-level switching current waveform is obtained as shown in the top subplot. After capacitor filtering, the current flowing to grid is very close to the sine wave, as shown in the second subplot. By setting $I_{sd}^{*}=1$ and $I_{sq}^{*}=0$, respectively, the unity power factor operation is achieved as shown in the third subplot, which is also reflected in the second plot, where the phase difference between line current and grid voltage is almost zero degree. The active power transferred to the grid is about 1.5 MW, as shown in the bottom subplot. Fig. 10 shows the steady state waveforms at 12 m/s. The stable DC-link current is increased and thus the output current amplitude of CSI is also increased,

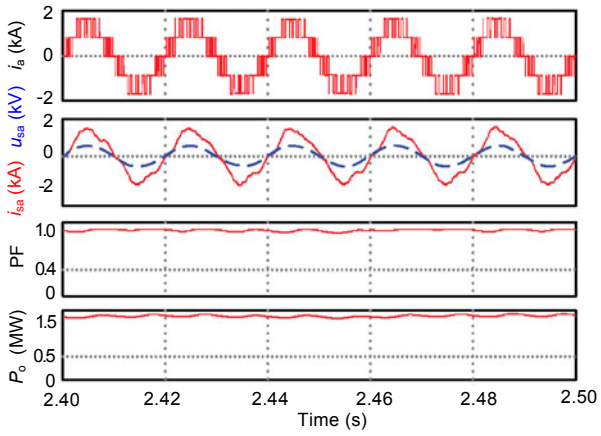

Fig. 9 Steady state waveforms at 9 m/s

as shown in the first and second subplots. Therefore, more active power (about 2.0 MW) will be transferred to the grid, as shown in the bottom subplot. The unity power factor operation is not changed for setting $I_{sq}^{*}=0$.

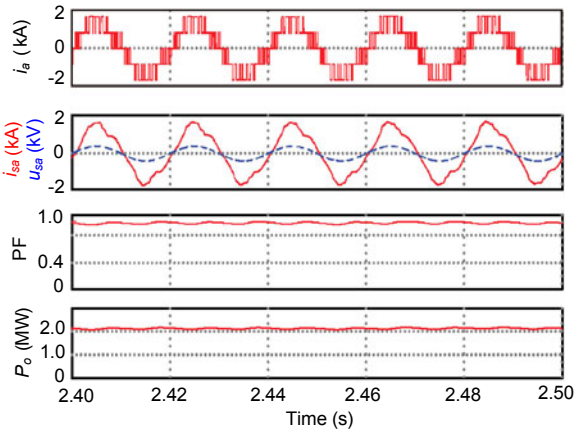

Fig. 10 Steady state waveforms at 12 m/s

Fig. 11 shows the leading displacement power factor generated at the grid side by independently regulating the reference components of the active and reactive powers, which are described as I_{sd}^{*} and I_{sq}^{*} in Fig. 6. By setting $I_{sd}^{*}=0.8$ and $I_{sq}^{*}=0.4$, the leading displacement power factor operation is produced. Fig. 11 shows the simulation waveforms at the wind speed of 9 m/s, and Fig. 12 shows the simulation waveforms at 12 m/s.

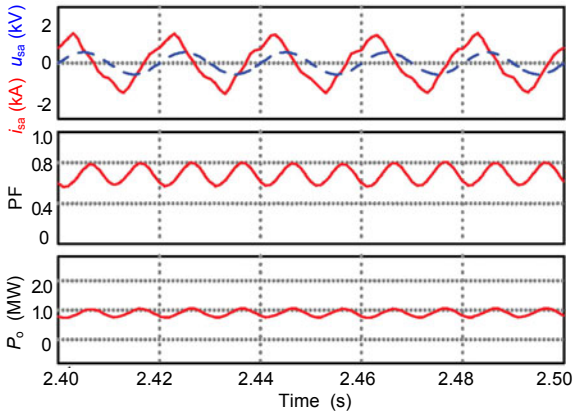

Fig. 11 Leading power factor operation at 9 m/s

Similarly, the lagging displacement power factor operation can be achieved in such a power conversion

system by setting $I_{sd}^{*}=0.8$ and $I_{sq}^{*}=-0.4$. The waveforms operated at two different wind speeds are shown in Figs. 13 and 14, respectively.

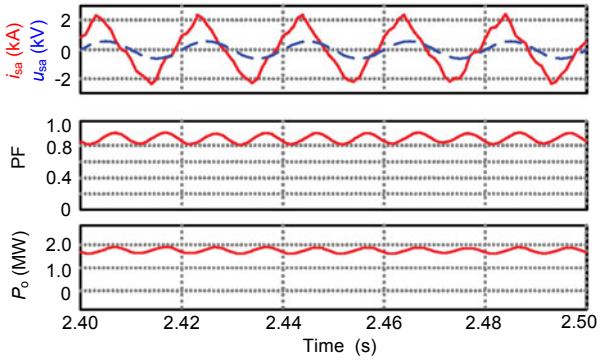

Fig. 12 Leading power factor operation at 12m/s

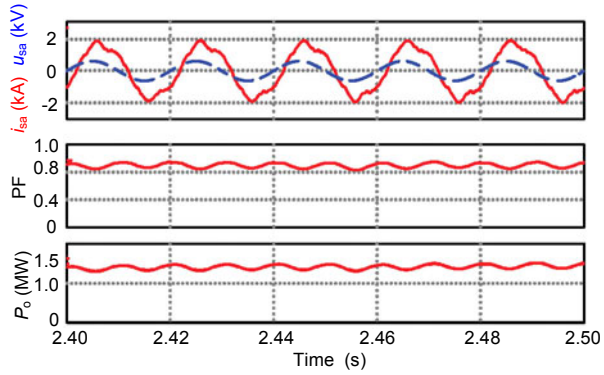

Fig. 13 Lagging power factor operation at 9 m/s

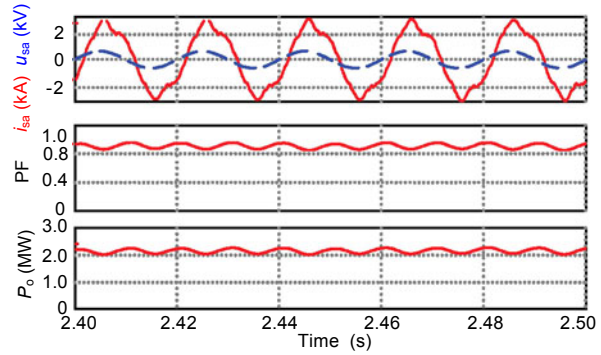

Fig. 14 Lagging power factor operation at 12 m/s

Fig. 15 shows the harmonic spectrum of the output current. The fundamental frequency is 50 Hz, and the switching frequency of CSI is 1050 Hz. The top subplot is the spectrum of the five-level switching current, in which the harmonic distribution mainly centralizes at 1050 Hz. The harmonic component situated in this frequency range can be eliminated by moderate filtering, and the spectrum after filtering is shown in the bottom subplot.

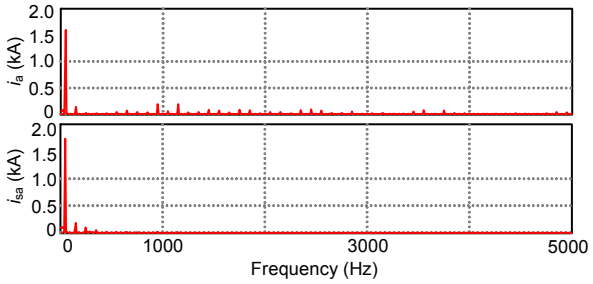

Fig. 15 Harmonic spectrum of output current

6 Conclusions

We propose a power conversion system used for PMSG based grid-connected WECS, composed of SVM CSR plus three-phase five-level CSI. On the generator side, an MPPT algorithm is implemented based on a generator rotation speed closed-loop regulation. DC-link current is controllable according to the varying wind speed via SVM CSR. On the grid side, a PD-PWM controlled three-phase five-level CSI is proposed to achieve relatively low line current harmonics. Its harmonic spectrum is close to that of a line-line voltage of five-level VSI. To conform with the grid-connected application, the active and reactive powers are regulated independently based on the grid voltage oriented control and PLL. The leading, unity, or lagging displacement power factor can be easily implemented on the grid side by presetting *d*- and *q*-axis reference currents, respectively. The proposed conversion system and control scheme are verified by a PSIM simulation.

References

Alizadeh, O., Yazdani, A., 2013. A strategy for real power control in a direct-drive PMSG-based wind energy conversion system. *IEEE Trans. Power Del.*, **28**(3):1297-1305. [doi:10.1109/TPWRD.2013.2258177]

Bai, Z., Ma, H., Xu, D., *et al.*, 2013. Control strategy with a generalized DC current balancing method for multimodule current-source converter. *IEEE Trans. Power Electr.*, **29**(1):366-373. [doi:10.1109/TPEL.2013.2252628]

Bao, J.Y., Bao, W.B., Zhang, Z.C., 2010a. Generalized multi-level current source inverter topology with self-balancing

current. *J. Zhejiang Univ.-Sci. C (Comput. & Electron.)*, **11**(7):555-561. [doi:10.1631/jzus.C0910605]

Bao, J.Y., Bao, W.B., Wang, S., *et al.*, 2010b. Multilevel current source inverter topologies based on the duality principle. Proc. 25th Annual IEEE Applied Power Electronics Conf. and Expo, p.1097-1100. [doi:10.1109/APEC.2010.5433367]

Chung, S.K., 2000. A phase tracking system for three phase utility interface inverters. *IEEE Trans. Power Electr.*, **15**(3):431-438. [doi:10.1109/63.844502]

Dai, J., Xu, D., Wu, B., 2009. A novel control scheme for current-source-converter-based PMSG wind energy conversion systems. *IEEE Trans. Power Electr.*, **24**(4):963-972. [doi:10.1109/TPEL.2008.2010259]

Dash, P.P., Kazerani, M., 2011. Dynamic modeling and performance analysis of a grid-connected current-source inverter-based photovoltaic system. *IEEE Trans. Sustain. Energy*, **2**(4):443-450. [doi:10.1109/TSTE.2011.2149551]

Dupczak, B.S., Perin, A.J., Heldwein, M.L., 2012. Space vector modulation strategy applied to interphase transformers-based five-level current source inverters. *IEEE Trans. Power Electr.*, **27**(6):2740-2751. [doi:10.1109/TPEL.2011.2177479]

Melício, R., Mendes, V.M.F., Catalão, J.P.S., 2010. Power converter topologies for wind energy conversion systems: integrated modeling, control strategy and performance simulation. *Renew. Energy*, **35**(10):2165-2174. [doi:10.1016/j.renene.2010.03.009]

Melício, R., Mendes, V.M.F., Catalão, J.P.S., 2011. Comparative study of power converter topologies and control strategies for the harmonic performance of variable-speed wind turbine generator systems. *Energy*, **36**(1):520-529. [doi:10.1016/j.energy.2010.10.012]

Nikolic, A., Jeftenic, B., 2010. Current source converter topologies for PMSG wind turbine applications. Proc. 14th Int. Power Electronics and Motion Control Conf., p.S14-27-S14-32. [doi:10.1109/EPEPEMC.2010.5606535]

Popat, M., Wu, B., Liu, F., *et al.*, 2012a. Coordinated control of cascaded current-source converter based offshore wind farm. *IEEE Trans. Sustain. Energy*, **3**(3):557-565. [doi:10.1109/TSTE.2012.2191986]

Popat, M., Wu, B., Zargari, N.R., 2012b. A novel decoupled interconnecting method for current-source converter-based offshore wind farms. *IEEE Trans. Power Electr.*, **27**(10):4224-4233. [doi:10.1109/TPEL.2012.2191982]

Popat, M., Wu, B., Zargari, N.R., 2013. Fault ride-through capability of cascaded current-source converter-based offshore wind farm. *IEEE Trans. Sustain. Energy*, **4**(2):314-323. [doi:10.1109/TSTE.2012.2223246]

Sahan, B., Araújo, S.V., Nöding, C., *et al.*, 2011. Comparative evaluation of three-phase current source inverters for grid interfacing of distributed and renewable energy systems. *IEEE Trans. Power Electr.*, **26**(8):2304-2318. [doi:10.1109/TPEL.2010.2096827]

Senturk, O.S., Helle, L., Munk-Nielsen, S., *et al.*, 2012. Power capability investigation based on electrothermal models of press-pack IGBT three-level NPC and ANPC VSCs for multimegawatt wind turbines. *IEEE Trans. Power Electr.*, **27**(7):3195-3206. [doi:10.1109/TPEL.2011.2182661]

Sharma, S., Singh, B., 2012. Control of permanent magnet synchronous generator-based stand-alone wind energy conversion system. *IET Power Electr.*, **5**(8):1519-1526. [doi:10.1049/iet-pel.2011.0367]

Singh, M., Khadkikar, V., Chandra, A., 2011. Grid synchronisation with harmonics and reactive power compensation capability of a permanent magnet synchronous generator-based variable speed wind energy conversion system. *IET Power Electr.*, **4**(1):122-130. [doi:10.1049/iet-pel.2009.0132]

Teshirogi, T., Nishikata, S., 2011. Effects of system parameters on the performance characteristics of a wind turbine generating system using a current-source thyristor inverter. *IEEE Trans. Ind. Appl.*, **47**(1):252-257. [doi:10.1109/TIA.2010.2091376]

Wang, J.C., Dai, J.Y., Wu, B., *et al.*, 2011. Megawatt wind energy conversion system with diode rectifier and multilevel current source inverter. Proc. IEEE Energy Conversion Congress and Exposition, p.871-876. [doi:10.1109/ECCE.2011.6063862]